GEOFIZIKA VOL. 16-17 1999-2000

Original scientific paper
UDC 550.341

Strong ground motion simulation using shear dislocation sources

J. P. Narayan

Department of Earthquake Engineering, University of Roorkee, Roorkee, India

Received 2 December 1999, in final form 15 November 2000

Paper presents the generation and implementation of various types of earthquake sources in a 2D finite difference grid. The procedure used for computing dislocations on the fault plane is identical to both well known kinematic and dynamic models, since it was calculated by solving the equation of motion taking into account the stress drop and the shear strength of the fault. This scheme is superior over the kinematic model because it calculates dislocation using stress drop instead of taking *a priori* dislocation pattern without any physical reasoning. Unlike the dynamic model, it does not require driving and resisting forces. The parsimonious staggered grid method was adopted instead of the conventional staggered grid since it requires less computational memory and enjoys the same advantage of being stable for larger Poisson's ratio, and free from spatial derivative of elastic parameters. Further, this scheme is flexible and allows a simple way of incorporating stress-free boundary condition. The algorithms were written for the simulation of P-SV and SH-waves propagation. The computed radiation patterns of the various earthquake sources for P-SV and SH-waves are in good agreement with the analytical radiation patterns. The effects of soil thickness and the velocity within it were studied in detail since they play an important role in the amplitude amplification, changes in signal duration, frequency content and mode conversion. Results depict that for the steeply incident waves, the impedance decrease and resonance effects control the amplitude amplification. The mode conversion at interfaces and multiple reflections in the surficial layer increase the signal duration.

Keywords: Strong ground motion, simulation, finite difference method

Introduction

The scale of socio-economic damage caused by an earthquake depends to a great extent on the characteristics of the strong ground motion (SGM), which in turn depend very much on the local site conditions. The realistic simulation and study of local site effects on the characteristics of SGM are therefore of prime importance in earthquake engineering. The study of effects of local geology on the characteristics of the SGM have been and continue to be, a field of active research since high frequency SGM is the least

understood area due to lack of ground motion records. The recent research in this area includes the works of Anderson et al. (1986), Mikumo and Miyatake (1987), Vidale and Helmberger (1987), Frankel and Vidale (1992), Kim et al. (1995), Boore and Joyner (1997) and Narayan (1998). In the past, most of the seismic simulations were done using explosive source (Virieux, 1984, 1986 and Kim et al., 1995). The point source simulation is not physically realisable since it can not explain the observed radiation patterns of different types of earthquake sources and is dominated by compressional wave only. The numerical implementation of double-couple sources were never completely presented for SGM simulation except by Vidale et al. (1985, 1987) and Coutant et al. (1995). Vidale et al. (1985, 1987) have used the Alterman and Karal (1968) and Alford et al. (1974) procedure but have not paid attention to numerical source description. The source implementation technique of Coutant et al. (1995) is relatively simpler, contains the complete description and is simpler than the technique of Vidale et al. (1985, 1987). However, Coutant et al. (1995) computations suffer a discrepancy in arrival time of horizontal and vertical components since they were computed at different locations separated by $\sqrt{2}$ times the grid size. The computation of shear dislocations based on displacement-stress relation seems physically more correct than the velocity-stress relation used by Coutant et al. (1995).

The elastodynamic equations are here approximated using the parsimonious staggering method of Ohminato and Chouet (1997) for P-SV and SH-waves. The numerical earthquake sources based on shear dislocation (such as dip-slip, strike-slip or explosive sources) were generated and implemented into the numerical grid using the recently developed technique of Coutant et al. (1995). The snapshots of particle displacement were taken at different times, so that different lobes corresponding to P- and S-waves and their polarity can be shown in the radiation pattern of a particular type of the source. The effects that velocity of elastic waves in the soil, the soil thickness and source type have on the characteristics of the SGM is studied in detail.

Parsimonious staggered grid scheme

The elastodynamic equations for P-SV and SH-waves are approximated using parsimonious staggered grid scheme (Luo and Schuster, 1990; Ohminato and Chouet, 1997). The superiority attributed to this scheme is that it is stable for a full range of Poisson's ratio and is free from the spatial derivative of elastic parameters over the second order centred difference scheme (Kelly et al., 1976). It requires less memory than both the standard staggered grid scheme (Virieux, 1984, 1986) and the Lax Wendroff scheme (Ram and Narayan, 1995). The stability criteria for this scheme are the same as for the mentioned schemes. The elastodynamic equations for the two dimensional P-SV wave propagation in heterogeneous media are:

$$\rho \frac{\partial^2 U}{\partial t^2} = \frac{\partial}{\partial x}(\sigma_{xx}) + \frac{\partial}{\partial z}(\sigma_{xz}) \tag{1}$$

$$\rho \frac{\partial^2 W}{\partial t^2} = \frac{\partial}{\partial x}(\sigma_{xz}) + \frac{\partial}{\partial z}(\sigma_{zz}) . \tag{2}$$

Here U and W are the particle displacements in the horizontal and vertical direction, ρ is the density of the medium. σ_{xx}, σ_{zz} and σ_{xz} are stress components. Time and spatial derivatives were replaced by the second order staggered grid differencing operator.

$$\rho_{l,m}\left(\frac{U_{l,m}^{n+1} + U_{l,m}^{n-1} - 2U_{l,m}^{n}}{\Delta t^2}\right) = \left(\frac{(\sigma_{xx})_{l,m}^{n} - (\sigma_{xx})_{l-1,m}^{n}}{\Delta x}\right) + \left(\frac{(\sigma_{xz})_{l,m+1}^{n} - (\sigma_{xz})_{l,m}^{n}}{\Delta z}\right) \tag{3}$$

$$\rho_{l,m}\left(\frac{W_{l,m}^{n+1} + W_{l,m}^{n-1} - 2W_{l,m}^{n}}{\Delta t^2}\right) = \left(\frac{(\sigma_{xz})_{l+1,m}^{n} - (\sigma_{xz})_{l,m}^{n}}{\Delta x}\right) + \left(\frac{(\sigma_{zz})_{l,m}^{n} - (\sigma_{zz})_{l,m-1}^{n}}{\Delta z}\right) \tag{4}$$

The stresses at time n used in equations (3) and (4) were computed using differenced stress-strain equations given below:

$$(\sigma_{xx})_{l,m}^{n} = (\lambda_{l,m} + 2\mu_{l,m})\left(\frac{U_{l+1,m}^{n} - U_{l,m}^{n}}{\Delta x}\right) + \lambda_{l,m}\left(\frac{W_{l,m+1}^{n} - W_{l,m}^{n}}{\Delta z}\right) \tag{5}$$

$$(\sigma_{zz})_{l,m}^{n} = \lambda_{l,m}\left(\frac{U_{l+1,m}^{n} - U_{l,m}^{n}}{\Delta x}\right) + (\lambda_{l,m} + 2\mu_{l,m})\left(\frac{W_{l,m+1}^{n} - W_{l,m}^{n}}{\Delta z}\right) \tag{6}$$

$$(\sigma_{xz})_{l,m}^{n} = \mu_{l,m}\left(\frac{U_{l,m}^{n} - U_{l,m-1}^{n}}{\Delta z} + \frac{W_{l,m}^{n} - W_{l-1,m}^{n}}{\Delta x}\right) . \tag{7}$$

λ, μ are Lame's parameters. Similarly, SH-wave approximation using parsimonious staggered grid scheme is given as,

$$\rho_{l,m}\left(\frac{V_{l,m}^{n+1} + V_{l,m}^{n-1} - 2V_{l,m}^{n}}{\Delta t^2}\right) = \left(\frac{(\sigma_{xy})_{l+1,m}^{n} - (\sigma_{xy})_{l,m}^{n}}{\Delta x}\right) + \left(\frac{(\sigma_{zy})_{l,m+1}^{n} - (\sigma_{zy})_{l,m}^{n}}{\Delta z}\right) \tag{8}$$

where V is particle displacement in the y-direction and other notation used has usual meaning. The stresses used in equation (8) at time n were computed using stress-strain relations:

$$(\sigma_{xy})^n_{l,m} = \mu_{l,m}\left(\frac{\partial V^n_{l,m}}{\partial x}\right) = \mu_{l,m}\left(\frac{V^n_{l,m} - V^n_{l-1,m}}{\Delta x}\right) \quad (9)$$

$$(\sigma_{zy})^n_{l,m} = \mu_{l,m}\left(\frac{\partial V^n_{l,m}}{\partial z}\right) = \mu_{l,m}\left(\frac{V^n_{l,m} - V^n_{l,m-1}}{\Delta z}\right) \quad (10)$$

The use of stress derivatives at time n in the equations (3), (4) and (8) is the reason for the parsimony. Δt is the time step and Δx and Δz are the grid intervals in the x- and z-directions, respectively. l and m are the grid indices in the x- and z-directions, and n is the time index.

Absorbing and stress-free boundary conditions

A physically justified stress-free boundary condition can not be realised by just putting λ and μ to zero. In this scheme only shear stress appears on the free surface of the unit material cell and normal stresses always remain embedded within the solid region. A unit material cell contains four finite difference grids. A stress-free boundary condition can be obtained just by setting $\mu = 0$ on the free surface. But by only setting $\mu = 0$ and $\lambda = 0$ in air does not ensure the vanishing of normal stress at the free surface (for details, please see Ohminato and Chouet, 1997). To avoid this, commonly used procedure to represent flat stress-free surface boundary is followed. A virtual cell above the boundary was taken with the same normal stress to that of the underlying cell but with the opposite polarity. In other words, the sum of these two anti-symmetric normal stresses across the boundary provides normal stress-free boundary condition. To avoid artificial reflections from the edges of the model, an absorbing boundary condition based on paraxial approximation of wave equation is applied (Clayton and Engquist, 1980).

Source implementation

Dislocations were computed using partial stress drop in the form of Ricker wavelet to control the initiation, propagation and stopping of the rupture as well as the frequency content in the source. The total area covered by the dislocation, once the entire wavelet was implemented, is the rupture area. This area will depend on the wave velocity and the duration of the wavelet. The two dimensional shear dislocation earthquake sources such as dip-slip, dip-slip at 45°, strike-slip and explosive source were implemented into the computational grid using the recently developed scheme by Coutant et al. (1995). Strike-slip rupture for P-SV wave was generated by applying the stress drop $\Delta\sigma(t)$ in x-direction only, dip-slip was generated by applying the stress drop $\Delta\sigma(t)$ in xz-plane only, dip-slip at 45° was generated by apply-

ing the stress drop $\Delta\sigma(t)$ in both the x and z-directions but with opposite polarities, and an explosive source was generated by applying the stress drop $\Delta\sigma(t)$ in both the x and z-directions with the same polarity. Similarly, strike-slip, dip-slip and explosive sources for SH-wave were generated by applying the stress drop $\Delta\sigma(t)$ in the xy-plane, zy-plane and in both the xy- and zy-planes, respectively.

The model parameters, namely Lame's constants, density and velocity, were assigned to each grid point after discretising the desired model into square grids. The snapshots were computed for P-SV and SH-waves radiation patterns of various types of shear dislocation sources at different times for a homogeneous model with equal Lame's parameters and a density of 10 GPa and 2.5 g/cm^3, respectively. The horizontal and the vertical radiation patterns of P-SV wave due to the strike-slip, dip-slips and explosion cases are shown in Figs. 1 and 2 at two times. Similarly, the radiation patterns of SH-

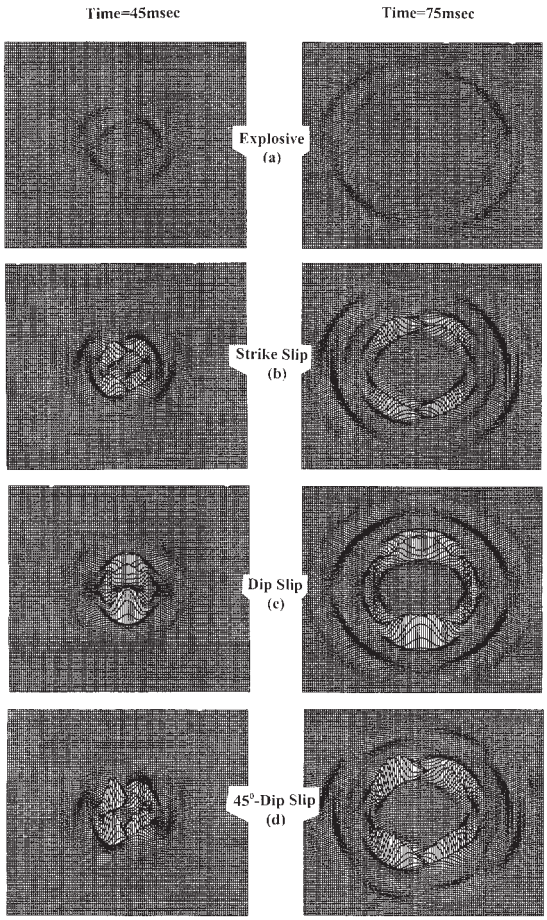

Figure 1. Horizontal component of radiation patterns of the point source and various shear dislocation sources of P-SV wave.

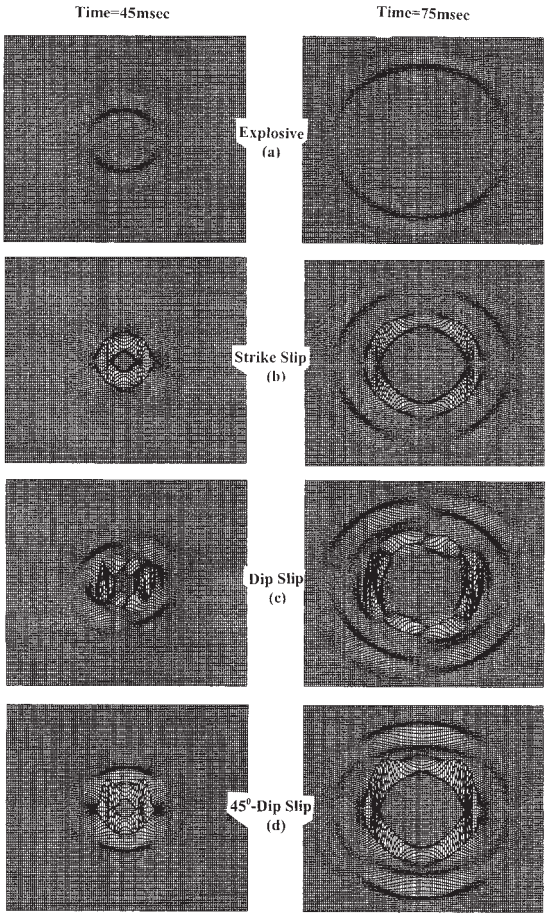

Figure 2. Vertical component of radiation patterns of the point source and various shear dislocation sources of P-SV wave.

wave due to the strike-slip, dip-slip and explosion cases are shown in Fig. 3 at two times. These computed radiation patterns corroborate with the analytical ones (Aki and Richards, 1980; Coutant et al., 1995) as well as with numerical radiation patterns computed by Vidale et al. (1985, 1987) in terms of number of P and S lobes and their respective polarities.

Numerical results

It has been found that the characteristics of the SGM in the basins are very much variable and complex and depend to a great extent on the soil type, its thickness and the geometry of the basin. Different models were therefore simulated using various shear dislocation sources, in order to study

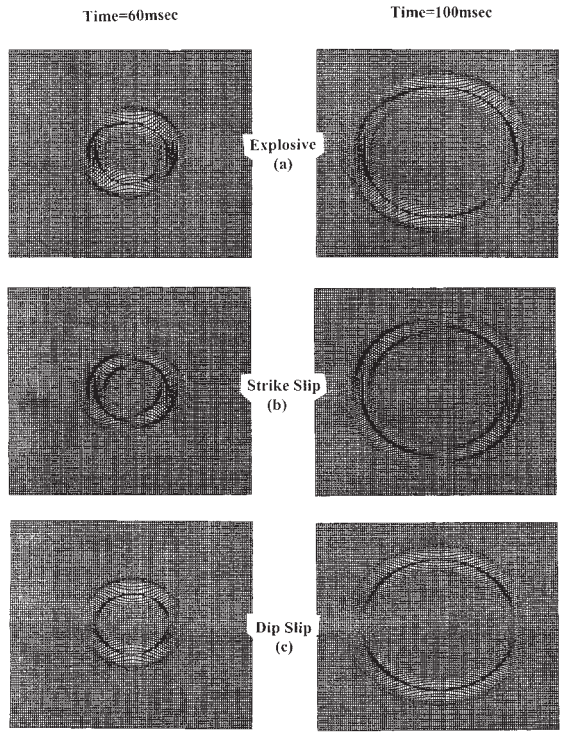

Figure 3. Radiation patterns of the point source and two shear dislocation sources of SH-wave.

the effects of velocity of elastic waves in soil, its thickness and the type of source on the characteristics of SGM. The time step, grid size and the dominant frequency of the source were taken as 0.3 ms, 20 m and 2 Hz, respectively. The parameters are listed in Table 1 for different models.

Table 1. Layer parameters for different models.

Thickness	Parameters	M1	M2	M3	M4
Soil cover	P-wave velocity (m/s)	1700	1664	2245	2928
100 meters	S-wave velocity (m/s)	500	800	1200	1600
	Density (g/cm^3)	1.70	2.00	2.20	2.40
	Poisson's ratio	0.455	0.350	0.300	0.250
Half space	P-wave velocity (m/s)	3464	3464	3464	3464
	S-wave velocity (m/s)	2000	2000	2000	2000
	Density (g/cm^3)	2.50	2.50	2.50	2.50
	Poisson's ratio	0.250	0.250	0.250	0.250

Effect of the source type

The horizontal and vertical components of the P-SV wave of the model M1 for strike-slip, dip-slip and dip-slip at 45° sources are shown in Figs. 4a and 4b, respectively. The responses were computed at 13 equidistant (1.0 km) locations, symmetrical to the epicentre. The maximum dynamic stress drop and focal depth in all the computations were 10 MPa and 6.5 km, respectively. The polarity reversals are in accordance with analytical radiation patterns. It is clear from these figures that shear component is dominating in the horizontal response and is comparable to the compressional component in the vertical response. Also, the particle displacement is almost zero at the epicentre in the horizontal response of strike slip and the 45° dip-slip sources

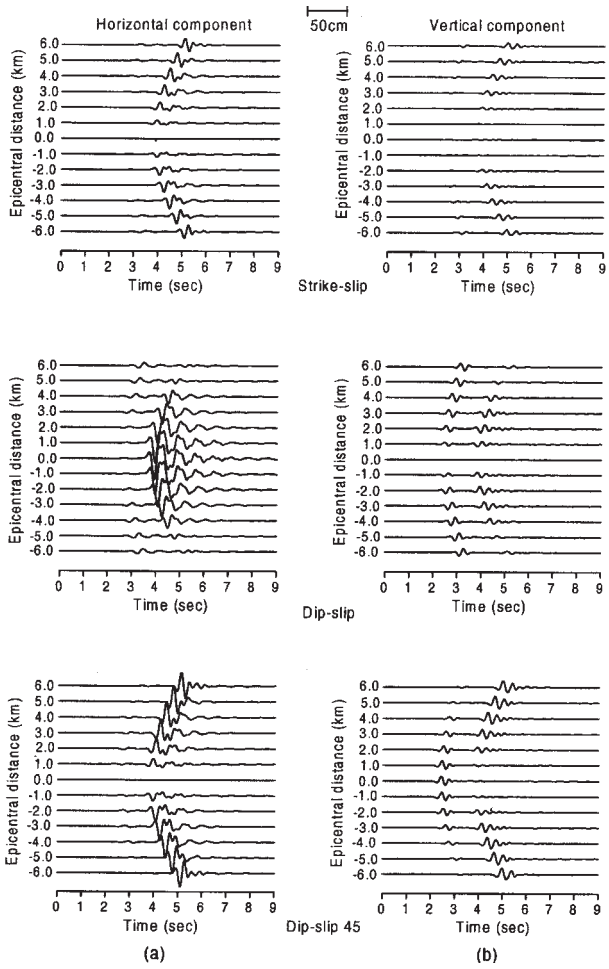

Figure 4. Strike-slip, dip-slip and dip-slip at 45°, horizontal (a) and the vertical (b) component of P-SV wave in the model M1.

as well as in the vertical response of the dip-slip and strike-slip sources. The high amplitude amplification factor and the increase in the signal duration in the epicentral region for the dip-slip response is due to sudden decrease of velocity and multiple reflection of waves in the surficial low velocity layer. The mode converted SV waves are visible just after the P-wave arrival in the case of the dip-slip source for large offset (Fig. 4a). The analysis of Figs. 4a and 4b yields that the dip-slip sources are the most damaging and the strike-slip sources are the least damaging in the epicentral region. The damage due to the dip-slip at 45° are in between these two cases. So, the pattern of damage also depends on the type of earthquake.

Effect of soil velocity

The response of two layered models with different velocity in the surficial layer were computed to find the effect of soil velocity on the characteristics of the SGM. Figs. 5a and 5b show the horizontal component of the particle displacement due to the dip-slip source at a depth of 6.5 km for the different models (Table 1) at two locations. Comparison of these figures depicts that at zero offset shear wave dominates as compared to the compressional wave but at the 6.0 km offset, the compressional wave amplitude is somewhat larger than that of the shear wave. The particle displacement due to the compressional wave (Fig. 5b) is maximum for the model M2 due to the lowest P-wave velocity in the surficial layer. Zero offset response depicts that as velocity in the surficial layer decreases both amplitude and duration increase due to the sudden decrease of the shear strength of the surficial layer. This means that the steeply incident wave due to a dip-slip source will be more damaging in the epicentral region, in low velocity layer.

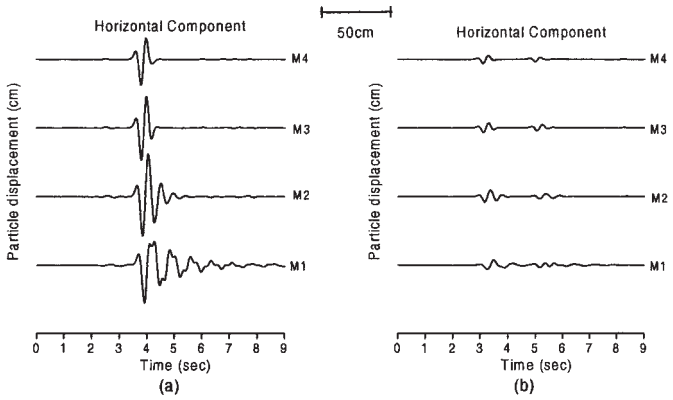

Figure 5. Dip slip horizontal responses of P-SV wave in different models at (a) zero offset and (b) 6.0 km offset.

Effect of soil thickness

The response of the model M1 for different thicknesses of the soil cover were computed to find the effect of thickness and resonance on the SGM characteristics. The response was computed with the dip-slip source at the 6.5 km depth. Figs. 6a and 6b show the zero offset and 6.0 km offset responses, respectively. Results depict that as the thickness of the surficial layer increases the duration of the signal increases too, but the amplitude amplification is not continuous for the different layer thicknesses. This may be due to the resonance effects. The higher frequencies are amplified when soil thickness is 40 m and lower frequencies are amplified when soil thickness is 80 m due to the resonance of the soil period with wave period. The amplitude amplification factor is very small when the layer thickness is only 20 m and amplification is almost constant for thickness more than 80 m. The offset responses also show the same effects.

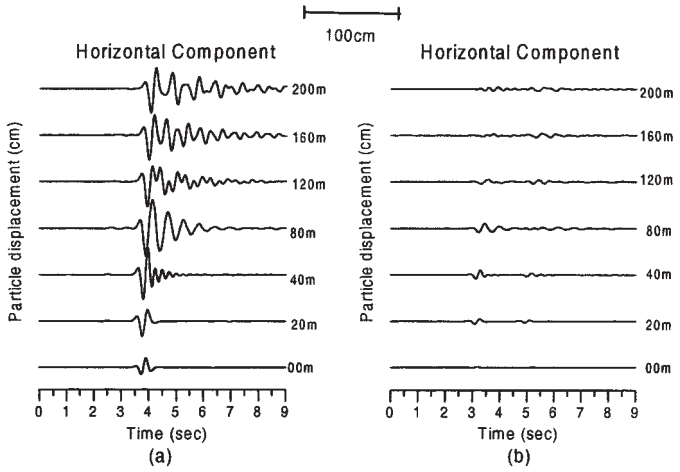

Figure 6. Dip-slip horizontal response of P-SV wave in the model M1 for different thicknesses of the soil cover at (a) zero offset and (b) 6.0 km offset.

Similarly, Fig. 7 shows the SH-wave response of the model M1 using dip-slip source at 2.6 km depth for different soil thicknesses. In this case the grid size, time step and dominant frequency were taken as 10 m, 0.003 s and 5 Hz, respectively. SH-wave response depicts the same pattern of amplitude amplification and duration increase as in the P-SV cases due to the variable thickness and resonance effects. Amplification factors for SH-wave for different soil thicknesses are given in Table 2. Amplification factor in the 1.5 km offset responses are smaller as compared to the zero offset responses.

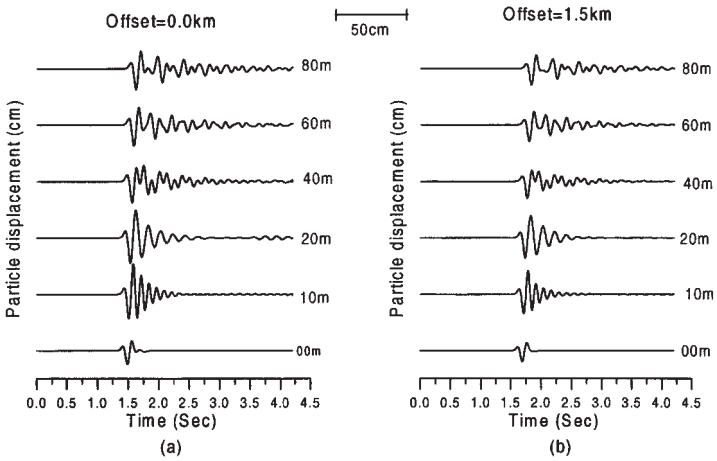

Figure 7. Dip-slip response of SH wave in the model M1 for different thicknesses of the soil cover at (a) zero offset and (b) 1.5 km offset.

Table 2. Amplification factor for different soil thicknesses.

Soil thickness	Amplification factor	
	Offset = 0.0 km	Offset = 1.5 km
0 m	1.00	1.00
10 m	2.32	2.26
20 m	2.23	2.19
40 m	1.49	1.47
60 m	1.60	1.58

The mode converted SV wave between the first arrival of P and SV wave are clearly visible in the offset responses of the model M1 (Fig. 5b). Now, it can be inferred from Figs. 4a, 5b and 6b that higher the Poisson's ratio in a layer the stronger will be the mode conversion and it further increases with the offset. A critical study of Figs, 5, 6 and 7 reveals that the signal duration and amplitude in a layer will be larger for large impedance contrast and large thickness. The amplitude will be further amplified when wave period matches the soil period.

Discussion and conclusions

Algorithms based on the parsimonious staggering scheme of Ohminato and Chouet (1997) were developed for P-SV and SH-waves, that reduce the

requirements for the computer memory. There is no need to save the stress components at two time steps in contrast to standard staggered grid scheme (Virieux, 1984, 1986). Also, this scheme is free from spatial derivatives of elastic parameters (Frankel et al., 1989). Parsimonious scheme is flexible and allows simple incorporating of the stress-free boundary conditions since only shear stress appears on the free surface. In the past, numerical excitation of the grids by double-couple sources were never completely presented, except for the implementation techniques of Vidale et al. (1985, 1987) and Coutant et al. (1995). The circular radiation pattern of explosive source is dominated by the compressional wave only, whereas the radiation patterns of earthquake sources change with the type of source. The opted source generation technique of Coutant et al. (1995) is simpler and more informative than the one of Vidale et al. (1985, 1987). The used staggering scheme is free from the discrepancy in the arrival time arising in the standard staggered grid scheme due to computation of velocity components at different locations (Coutant et al., 1995). The computation of shear dislocations based on the displacement-stress relation seems physically more correct than the velocity -stress relation used by Coutant et al. (1995). The computed radiation patterns of the various shear dislocation sources are in good agreement with the analytical as well as numerical radiation patterns computed by Vidale and Helmberger (1987).

It was concluded that the lower shear strength in the surficial layer facilitates the amplitude amplification, mode conversion and increase in signal duration. It was also inferred that mode conversion increase with increase of Poisson's ratio and the offset. The simulated results for different thickness of soil cover depict that as the thickness of the layer increases the signal duration increases too. The amplification factor is not continuous due to the resonance effects. The damage pattern very much depends on the type of source. Dip-slip source is more damaging and strike-slip source is the least damaging in the epicentral region. This type of study will be the most useful for the purpose of earthquake engineering in the areas where there are no ground motion records. Also, we have not to wait for the impending earthquakes to occur. The main purpose of developing these algorithms was to generate appropriate earthquake source model based on the controlled physical parameters and to study the effects of local site conditions on the characteristics of the ground motion.

Acknowledgements – Financial support by Indian National Science Academy (INSA), New Delhi, and University Grants Commission (UGC), New Delhi, is thankfully acknowledged.

References

Aki, K. and Richards, P. G. (1980): Quantitative seismology: Theory and methods, San Francisco, W. H. Freeman.

Alford, R. M., Kelly, K. R. and Boore, D. M. (1974): Accuracy of finite difference modelling of the acoustic wave equation, Geophysics, **39**, 834–842.

Anderson, J. G., Bodin, P., Brune, N. J., Prince, J., Singh, S. K., Quaas, R. and Onate, M. (1986): Strong ground motion from the Michoacan, Mexico earthquake, Science, **233**, 1043–1049.

Boore, D. M. and Joyner, W. B. (1997): Site amplification of generic rock sites, Bulletin of the Seismological Society of America, **87**, 327–341.

Clayton, R. W. and Engquist, B. (1980): Absorbing side boundary conditions for wave equation migration, Geophysics, **45**, 895–904.

Coutant, O., Virieux, J. and Zollo, A. (1995): Numerical source implementation in a 2D finite difference scheme for wave propagation, Bulletin of the Seismological Society of America, **85**, 1507–1512.

Frankel, A. (1989): A review of numerical experiments on seismic wave scattering, Pure and Applied Geophysics, **131**, 639–689.

Frankel, A. and Vidale, J. (1992): A three-dimensional simulation of seismic waves in the Santa Clara Valley, California, from a Loma Prieta aftershock, Bulletin of the Seismological Society of America, **82**, 2045–2074.

Kelly, K. R., Ward, R. W., Trietel S. and Alford, R. M. (1976): Synthetic seismograms: A finite difference approach, Geophysics, **41**, 2–27.

Kim, O. B., James, C. P. and Schuster, G. T. (1995): Simulation of 3D elastic wave propagation in the Salt Lake basin, Bulletin of the Seismological Society of America, **85**, 1688–1710.

Luo, Y. and Schuster, G. (1990): Parsimonious staggered grid finite differencing of the wave equation, Geophysical Research Letters, **17**, 155–158.

Mikumo, T. and Miyatake, T. (1987): Numerical modelling of realistic fault rupture process. In *Seismic Strong Motion Synthetics* (Bolt, B. A., ed.), Academic Press, Orlando, USA.

Narayan, J. P. (1998): Numerical strong ground motion simulation and study of local site effects, Proceedings of the 11th Symposium on Earthquake Engineering, Dec. 17–19, University of Roorkee, Roorkee, India.

Ohminato, T. and Chouet, B. A. (1997): A free surface boundary condition for including 3D topography in the finite difference method, Bulletin of the Seismological Society of America, **87**, 494–515.

Ram, A. and Narayan, J. P. (1995): Simulation of the hydrocarbon structures using the P-SV wave solution, Pure and Applied Geophysics, **144**, 59–77.

Vidale, J. E., Helmberger, D. V. and Clayton, R. W (1985): Finite difference seismograms for SH-waves, Bulletin of the Seismological Society of America, **75**, 1765–1782.

Vidale, J. E. and Helmberger, D. V. (1987): Path effect in strong motion seismology. In *Seismic Strong Motion Synthetics* (Bolt, B. A., ed.), Academic Press, Orlando, USA.

Virieux, J. (1984): SH wave propagation in heterogeneous media, velocity stress finite-difference method, Geophysics, **49**, 1933–1957.

Virieux, J. (1986), P-SV wave propagation in heterogeneous media, velocity stress finite-difference method, Geophysics, **51**, 889–901.

SAŽETAK

Simulacija snažne trešnje tla pomoću smičnih dislokacijskih izvora

J. P. Narayan

U radu je razmotreno zračenje različitih vrsta potresnih izvora pomoću metode konačnih razlika u dvodimenzionalnoj mreži. Rabljeni postupak daje jednake rezultate kao dobro poznati kinematički i dinamički modeli, jer se račun provodi rješavanjem jednadžbi gibanja uzimajući u obzir pad napetosti i otpornost na smicanje po rasjednoj plohi. Rabljena je shema superiorna kinematičkom modelu jer se pomaci računaju pomoću pada napetosti umjesto korištenjem unaprijed zadane razdiobe pomaka bez ikakve fizikalne podloge. Prednost u odnosu na dinamički model je da nije potrebno pretpostaviti nikakvu vanjsku silu. Rabljena shema je fleksibilna i omogućuje jednostavno uvođenje rubnih uvjeta na granicama modela. Napisani su algoritmi za simulaciju rasprostiranja P-SV i SH valova. Izračunate razdiobe pomaka za razne potresne izvore u suglasju su s analitičkim rješenjima. Detaljno je razmotren utjecaj debljine površinskog sloja i pretpostavljene brzine rasprostiranja elastičkih valova, koji imaju velik utjecaj na amplifikaciju, trajanje signala, frekventni sadržaj i konverziju modova. Rezultati ukazuju da je amplifikacija u slučaju strmo-upadajućih valova kontrolirana smanjenjem impedancije i rezonantnim efektima. Konverzija modova na diskontinuitetima i višestruke refleksije povećavaju trajanje signala.

Ključne riječi: Snažna trešnja tla, simulacija, metoda konačnih razlika

Author's address: J. P. Narayan, Department of Earthquake Engineering, University of Roorkee, Roorkee-247 667, India. e-mail: jaypnfeq@rurkiu.ernet.in